

RSC Advances



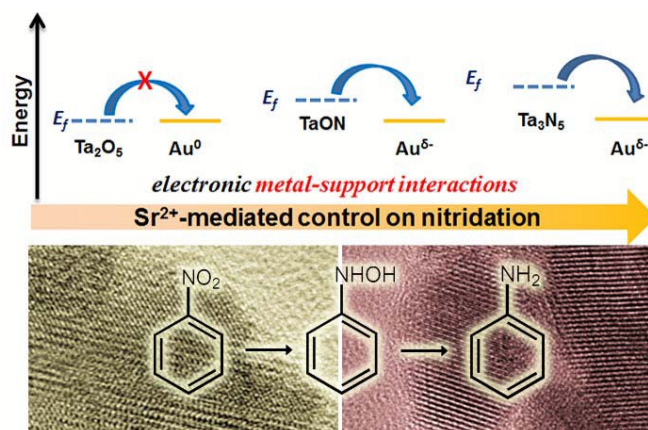
This is an *Accepted Manuscript*, which has been through the Royal Society of Chemistry peer review process and has been accepted for publication.

Accepted Manuscripts are published online shortly after acceptance, before technical editing, formatting and proof reading. Using this free service, authors can make their results available to the community, in citable form, before we publish the edited article. This *Accepted Manuscript* will be replaced by the edited, formatted and paginated article as soon as this is available.

You can find more information about *Accepted Manuscripts* in the [Information for Authors](#).

Please note that technical editing may introduce minor changes to the text and/or graphics, which may alter content. The journal's standard [Terms & Conditions](#) and the [Ethical guidelines](#) still apply. In no event shall the Royal Society of Chemistry be held responsible for any errors or omissions in this *Accepted Manuscript* or any consequences arising from the use of any information it contains.

Graphic abstract



Optimized metal-support interactions was achieved on ionothermally prepared tantalum (oxy)nitrides with controlled nitridation, and the as-formed $Au^{\delta-}$ species promoted by TaON are efficient for nitrobenzene hydrogenation due to its moderated adsorption of substrates.



Journal Name

ARTICLE

Controlled Nitridation of Tantalum (Oxy)Nitride Nanoparticles towards Optimized Metal-Support Interactions with Gold Nanocatalysts

Received 00th January 20xx,
Accepted 00th January 20xx

DOI: 10.1039/x0xx00000x

www.rsc.org/

Xiaoyun Yang^a, Sina He^a, Yijin Shu^a, Zhangping Shi^b, Yulin Guo^a, Qingsheng Gao*^a and Yi Tang^b

The electron regulation on supports can vary metal-support interactions with loaded metals in heterogeneous catalysis. In this paper, a facile Sr²⁺-mediated ionothermal route was introduced to control the nitridation degree in tantalum (oxy)nitrides, resulting in varied electronic properties and optimized interactions with gold nanocatalysts. A new mechanism was proposed that the formation of SrTa₄O₁₁ intermediates facilitated the replacement of O by N in controlled nitridation, and more importantly avoided undesired over-nitridation. As expected, the TaON support with defined nitridation promoted electronic metal-support interactions to generate Au^{δ-} species, which was highly active for the thermal hydrogenation of nitrobenzene due to the moderated adsorption and effective activation on Au^{δ-} in Au/TaON. This work elucidated the optimized metal-support interactions achieved on controllably nitridated supports, opening up new opportunities for the development of efficient nanocatalysts.

1. Introduction

Metal nitrides are a class of important functional materials in catalysis, refractory ceramics, sensing, electrochemistry, and optoelectronics, due to their rich physicochemical properties associated with the tunable interactions between metal and nitrogen.¹⁻⁴ On one hand, the enlarged metal-metal bonds in the alloy phases of many metal nitrides lead to the reduced density of unoccupied d-orbitals around Fermi level, and the noble-metal-like catalytic behaviours.⁵⁻⁸ On the other hand, the electron transfer from metal to nitrogen will oppositely increase the density of unoccupied d-orbitals.⁸ Thus, the synergy of the above two functions varies the electronic features and catalytic performance of metal nitrides. Many nitrides active for hydrogen-involving catalytic reactions have been developed,^{5,7} and very recently, they are discovered as prominent supports due to the rich interactions with loaded metals.^{9,10} As evidence in catalytic nitroarene hydrogenation,^{11,12} the metal-support interactions with gold are promoted by Mo₂N supports. In comparison with the counterparts of metal oxides,^{13,14} several advantages are highlighted in nitride-based supports, e.g., noble-metal-like d-

band structures, tailorable electron properties, and tunable metal-support interactions.⁷ Regarding the prevailing Mott-Schottky effects in the interfaces between metals and semiconductors,¹⁵ the electron regulation on nitrides is desired to further optimize the metal-support interactions, which is however rarely reported.

Introducing N into metal oxides usually brings narrowed band-gap and increased Fermi level as a result of the synergetic effects of both alloying and electron-transfer,^{16,17} which indicates a facile electron-manipulation by controlled nitridation. In the case of tantalum (oxy)nitrides, the smaller band-gap energy (vs. Ta₂O₅) enables them as novel visible-light photocatalysts,^{17,18} and the rich defect and tunable valence state are further proved promising for nonphotocatalytic hydrogenation and oxidation.¹⁹⁻²¹ It's more important that tantalum (oxy)nitrides can be utilized as promising catalyst supports. Their increased Fermi level and tunable electron features would promote the electronic interactions with metals, showing advantages in comparison with Ta-oxides.²²⁻²⁴ To achieve the optimized metal-support interactions in efficient catalysis, the controlled nitridation in tantalum (oxy)nitrides is highly demanded, however, it suffers easy over-nitridation to by-products of Ta₃N₅, Ta₄N₅, and even TaN during high-temperature synthesis.^{25,26}

Nitridation utilizing organic-inorganic hybrid precursors provides the tailored generation of nitrides.^{8,27} Herein, a facile Sr²⁺-mediated route is conducted to accomplish the controlled nitridation in tantalum (oxy)nitride nanoparticles, which are mono-dispersed, well-separated and mostly single crystalline. A new mechanism via tantalate intermediate is proposed for the controlled nitridation. The formation of SrTa₄O₁₁, in which Ta-O bonds are weakened by Sr²⁺, ensures the generation of

^a Department of Chemistry, Jinan University, 510632, Guangzhou, China
E-mail: tqsgao@jnu.edu.cn

^b Department of Chemistry, Shanghai Key Laboratory of Molecular Catalysis and Innovative Materials, Laboratory of Advanced Materials and Collaborative Innovation Center of Chemistry for Energy Materials, Fudan University, 200433, Shanghai, China.

† Footnotes relating to the title and/or authors should appear here.
Electronic Supplementary Information (ESI) available: additional characterization of SEM, TEM, XRD, TGA/DSC, IR, N₂ isothermal sorption and CO uptake. See DOI: 10.1039/x0xx00000x

pure TaON or Ta₃N₅ at mild temperature, and avoids over-reactions. This innovation can be extended to other ionothermal system utilizing a wide range of alkaline-earth-metal salts, and can well address the remaining puzzlements in the previous work. For example, the previous Ca²⁺-assisted mechanism associated with the controlled NH₃-release from Ca²⁺-chelated urea is controversial,²⁸ because urea decomposes much earlier than nitridation reactions upon heating. The new mechanism via tantalate intermediates makes an obvious progress in the understanding of essential effects of ionic solvents. More importantly, it is discovered for the first time that such controlled nitridation obviously varies the electronic properties of tantalum (oxy)nitrides to express electronic metal-support interactions with gold for catalytic hydrogenation. In the probe reaction of nitrobenzene (NB) reduction under thermal condition, remarkably improved activity and optimized aniline (AN) selectivity are achieved over Au/TaON, as compared with those on Au/Ta₂O₅ and Au/Ta₃N₅. This is ascribed to the suitable adsorption and effective activation of substrates by moderately negative Au^{δ-} on TaON support.

2. Experimental section

2.1 Catalysts preparation

In a typical ionothermal procedure, 0.250 g of TaCl₅ powder was added to 2 mL of methanol, followed by adding 0.103 of SrCO₃. After a varied amount of urea was added, the solution was let dry to gel under stirring at room temperature. The precursor was transferred into an oven and kept under N₂ flow (500 mL min⁻¹) for 2.0 h in order to remove air before heating, and then was heated to 700 °C with a ramping rate of 5 °C min⁻¹, being held for 5 h. After treating the as-received powders with 1 M HCl (aq.) for 48 hours to remove Sr-species, tantalum (oxy)nitrides nanoparticles were obtained. Other ionothermal synthesis employing Ba²⁺, Ca²⁺ and Mg²⁺ was carried out via the same processes, except that SrCO₃ was replaced by BaCO₃ (0.138 g), CaCO₃ (0.070 g) and MgCO₃ (0.059 g), respectively.

Meanwhile, Ta₂O₅ nanoparticles used for control catalytic tests were synthesized via traditional reverse homogeneous precipitation. 0.360 g of TaCl₅ was dissolved in 5 mL of methanol, and then, 15 mL of NH₃·H₂O (19%, aq.) was added. After stirring for 1 hour, the white precipitate was washed with water and ethanol. After heating at 750 °C for 5h under air, Ta₂O₅ nanoparticles were received.

A typical deposition-precipitation procedure was employed to prepare Au/Ta₂O₅, Au/TaON, and Au/Ta₃N₅ catalysts. Briefly, Ta-based nanoparticles were dispersed with the aqueous solution of HAuCl₄ (4.856×10⁻³ mol L⁻¹), and pH was adjusted to 9.0 by dropwise addition of 0.25 M NH₃·H₂O (aq.). After stirring for 6 hours and aging for another 2 hours, the catalyst was washed with deionized water for five times and then dried at 50 °C overnight, followed by a careful reduction with a stream of 5 vol% H₂/Ar at 300 °C for 2 hours.

2.2 Physical measurement

X-ray diffraction (XRD) analysis was performed on Bruker D8 diffractometer using Cu Kα radiation (λ = 1.54056 Å). Scanning electron microscopy (SEM) and transmission electron microscopy (TEM) investigations were taken on a ZEISS ULTRA55 and a JEOL JEM 2100F, respectively. Energy dispersive spectrum (EDS) was carried out on a JEOL JEM 2100F. X-ray photoelectron spectroscopy (XPS) analysis was processed on a Perkin-Elmer PHI X-tool, using C 1s (B. E. = 284.6 eV) as a reference. The N content in TaON and Ta₃N₅ was determined by CHNS elemental analysis using a Vario EL Elementar, and the Au loading was investigated by an inductively coupled plasma-atomic emission spectroscopy (ICP-AES). Thermogravimetric analysis coupling with differential scanning calorimeter (TGA/DSC) was tested on NETZSCH STA449F3 under N₂ flow. The UV-vis diffuse reflection spectra (UV-vis DRS) were carried out on Varian Cary 5000 at room temperature. IR spectra were collected with a Nicolet 6700 FTIR spectrometer. The B.E.T. specific surface areas were determined by adsorption-desorption of nitrogen at liquid nitrogen temperature, using a Micromeritics TriStar 3000 equipment, degassing at 300 °C. Hydrogen temperature-programmed reduction (H₂-TPR) and CO pulse adsorption were both conducted on the XianQuan instrument TP 5076.

2.3 Catalytic test of NB hydrogenation

Nonphotocatalytic test was carried out in a 100 mL stainless steel autoclave, in which 40 mg of catalyst, 0.5 mmol of NB, 6.0 mmol of formic acid (FA), 5.0 mL of H₂O and 5.0 mL of EtOH were loaded. The reactor was purged with 0.5 MPa N₂. The reaction was conducted at 80 °C for 2.5 hours, with the stirring of 500 rpm. The products were analyzed by Shimadzu HPLC LC-20A with a RID detector. To further study the catalytic mechanism, a series of control tests by photo-excitation were conducted in a stainless steel autoclave with a quartz window under the irradiation of Xe lamp (λ > 200 nm adopted for Au/Ta₂O₅, and λ = 400 ~ 800 nm for Au/TaON and Au/Ta₃N₅). Meanwhile, in the catalytic decomposition of FA over supported Au, the liquid product was analyzed by Shimadzu HPLC LC-20A, and the gas product was tested by Shimadzu GC-2014C.

3. Results and discussion

3.1 Characterization of TaON and Ta₃N₅ nanoparticles

In the presence of SrCl₂, the controllable nitridation of tantalum can be achieved via simply changing the molar ratio of urea to Ta (R_{U/Ta}) in starting gels, followed by calcination at 700 °C under N₂ flow and a treatment with HCl. As confirmed by XRD investigation (Fig. 1), the products evolve from Ta₂O₅ to TaON and finally Ta₃N₅ as R_{U/Ta} is increased from 1.0 to 7.0, accompanied with the visible color changing from white to yellow and finally red. For a R_{U/Ta} of 2.0, TaON products are obtained, namely γ-TaON (ICDD No.: 01-076-3258) and β-TaON (ICDD No.: 04-010-4352); while, Ta₃N₅ (ICDD No.: 01-089-5200) is harvested as R_{U/Ta} is 7.0, indicating the well-defined nitridation. The comparison of these products with the

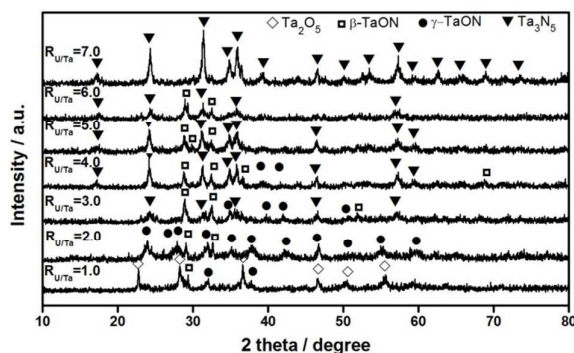


Fig. 1 XRD patterns of products obtained in the presence of Sr^{2+} with the $R_{\text{U}/\text{Ta}}$ from 1.0 to 7.0.

standard patterns from ICDD database is further shown in ESI[†] as Fig. S1.

Furthermore, the SEM investigation shows that all the products are in form of well-defined nanoparticles (Fig. S2 in ESI[†]). Representatively, Fig. 2a and 2b display the SEM images of TaON and Ta_3N_5 , which are obtained with a typical $R_{\text{U}/\text{Ta}}$ of 2.0 and 7.0, respectively. They are about 20–30 nm in diameter. In the TEM images (Fig. 2c and 2d), TaON can be distinguished by the clear (110) and (200) lattice fringes, while Ta_3N_5 is confirmed by the (110) and (402). The EDS obtained on the both of above nanoparticles confirm the complete removal of SrCl_2 by a treatment with 1 M HCl (Fig. S3 in ESI[†]). Additionally, such TaON and Ta_3N_5 exhibit a surface area of 21.3 and 25.6 m^2/g , respectively (Table S1 in ESI[†]).

XPS analysis further gives clear evidence about TaON and Ta_3N_5 with varied electronic structures (Fig. 3). With the introduction of N, TaON presents the obviously shifted peaks of Ta 4f $_{7/2}$ and 4f $_{5/2}$ at the lower binding energies of 26.0 and

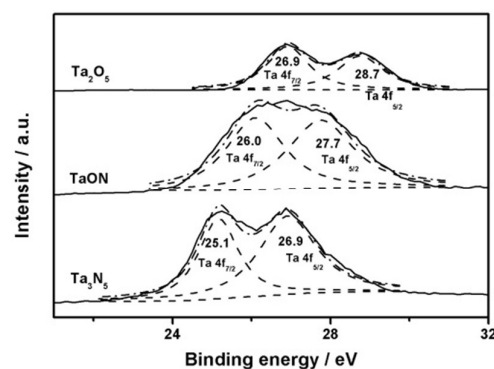


Fig. 3 Ta 4f XPS spectra of Ta_2O_5 , TaON and Ta_3N_5 .

27.7 eV, respectively, as compared with those located at 26.9 and 28.7 eV in Ta_2O_5 .²⁹ This is associated with the lower electronegativity of N than that of O, as well as the consequently favored electron transfer from N to Ta. In this way, Ta_3N_5 displays the further decreased binding energy of 25.1 and 26.9 eV for Ta 4f $_{7/2}$ and 4f $_{5/2}$, respectively. Meanwhile, the red-shifted absorption bands of TaON and Ta_3N_5 nanoparticles in UV/Vis DRS (Fig. S4a in ESI[†]), in comparison with those for Ta_2O_5 , indicate the narrowed band-gap due to nitridation. According to previous reports,²⁹ the valence band in tantalum (oxy)nitrides, mainly contributed by O2p and N2p orbitals, ascends from -7.93 eV in Ta_2O_5 , to -6.6 eV in TaON and -6.02 eV in Ta_3N_5 , bringing about obviously increased Fermi level with the increased nitridation degree (Fig. S4b in ESI[†]).

3.2 Mechanism for the controlled nitridation of tantalum.

Sr^{2+} is found indispensable for the effective control over nitridation. In the absence of Sr^{2+} , uncontrolled nitridation usually results in undesired mixtures (Fig. 4). With a low $R_{\text{U}/\text{Ta}}$ of 1.0, un-nitridated Ta_2O_5 and over-nitridated Ta_3N_5 are observed along with desired TaON. As $R_{\text{U}/\text{Ta}}$ is increased from 2.0 to 7.0, the mixture of TaON and Ta_3N_5 unfortunately remains, and at a high $R_{\text{U}/\text{Ta}}$ of 8.0, another by-product of TaN emerges. Given the rich interactions arising from ionic solvents

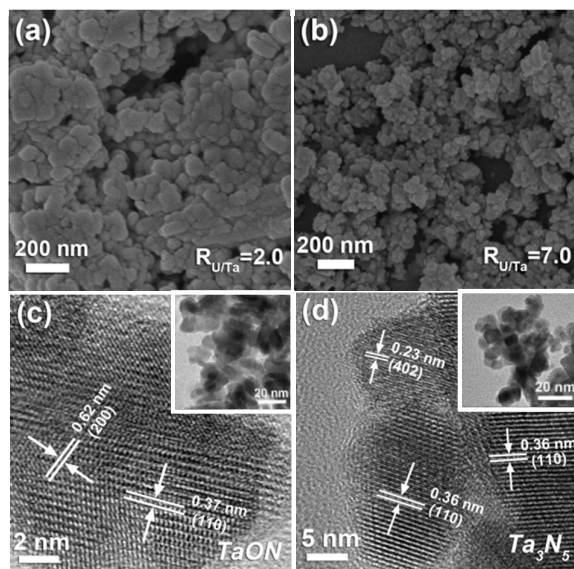


Fig. 2 (a, b) SEM and (c, d) TEM images of (a, c) TaON and (b, d) Ta_3N_5 NPs, harvested at $R_{\text{U}/\text{Ta}} = 2.0$ and 7.0, respectively.

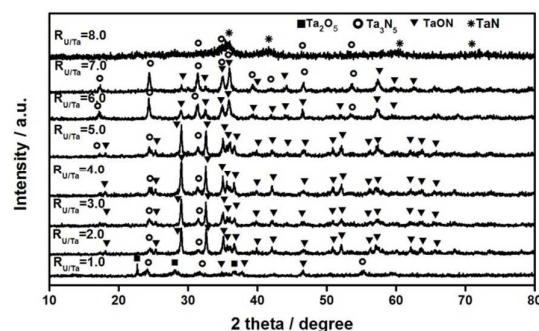


Fig. 4 XRD patterns of products obtained in the absence of Sr^{2+} with the varied $R_{\text{U}/\text{Ta}}$ ratio from 1.0 to 8.0.

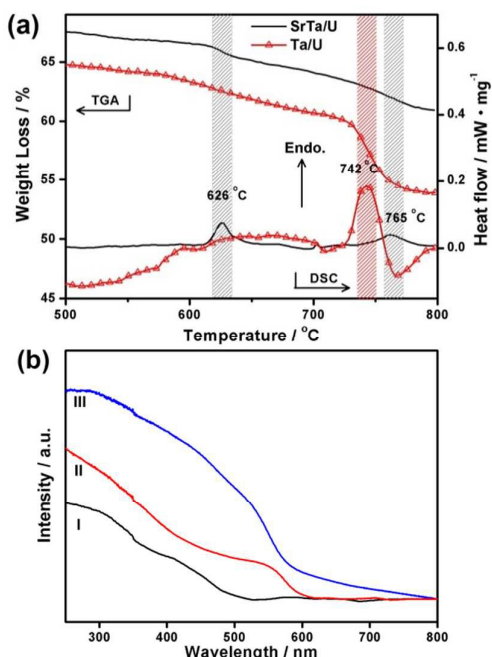


Fig. 5 (a) TGA/DSC curves of SrTa/U and Ta/U with $R_{U/Ta}$ of 2.0, focusing on the evolution upon 500 °C. (b) UV-vis DRS of products taken from TGA/DSC analysis at (I) 650 and (II) 800 °C in SrTa/U ($R_{U/Ta} = 2.0$), and at (III) 800 °C in Ta/U ($R_{U/Ta} = 2.0$).

in ionothermal routes,³⁰ the role of Sr^{2+} should be taken into account for the controlled generation of TaON and Ta_3N_5 nanoparticles.

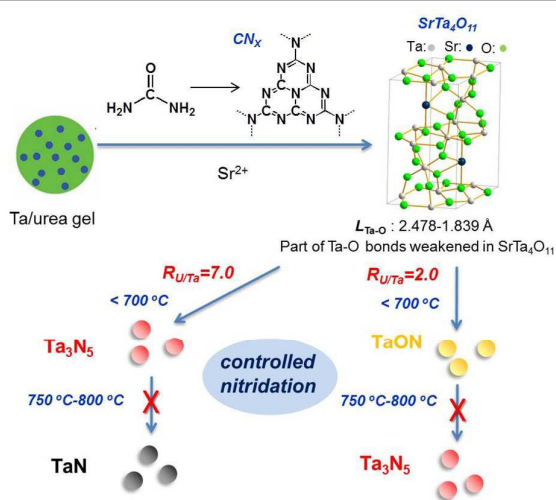
As the ionothermal processes were conducted at lower temperature (550 °C) or with a lower flow rate of carrier N_2 (100 mL min^{-1}) than that for a typical procedure (700 °C and 500 mL min^{-1}), in which nitridation reactions were depressed,³¹ the intermediate of $SrTa_4O_{11}$ (ICDD No.: 01-083-0608) was received (Fig. S5 in ESI†). This observation indicates the strong interactions between Sr and Ta in the form of strontium tantalate during ionothermal synthesis. According to the crystalline data of $SrTa_4O_{11}$ and Ta_2O_5 (Fig. S6 in ESI†), some weakened Ta-O bonds in $SrTa_4O_{11}$ are suggested by the extended length in a wider range (1.839 ~ 2.478 Å) than that in Ta_2O_5 (1.839 ~ 2.126 Å). This predicts the easier breaking of Ta-O in strontium tantalate under nitridation, and the promoted replacement of O atoms by N, as verified by the following thermal analysis.

The TGA/DSC analysis under N_2 atmosphere was conducted on the similar gel precursors with and without Sr^{2+} , which were denoted as SrTa/U and Ta/U, respectively (Fig. S7 in ESI†). The same $R_{U/Ta}$ of 2.0 was adopted. To elucidate the nitridation reactions, we focus on the evolution in TGA/DSC over 500 °C (Fig. 5a). Noticeably, the nitrogen source at such high temperature is CN_x derived from urea,^{20,32} whose presence has been verified by IR spectra (Fig. S8 in ESI†). The SrTa/U precursor shows a weight loss and an endothermic peak around 626 °C, and another evolution near 765 °C. The samples taken from TGA/DSC at 650 and 800 °C respectively

exhibit the typical absorption band-edges of TaON (490 nm) and Ta_3N_5 (600 nm) in UV-vis DRS (Fig. 5b). It is indicated that the reactions around 626 °C in TGA/DSC would be associated with the nitridation to TaON, at which point the further reaction to Ta_3N_5 requiring higher temperature of 765 °C is avoided. However, Ta/U without Sr^{2+} only presents a drastic weight loss and an obvious endothermic peak around 742 °C, consistent with the synthetic procedure requiring calcination at 775 °C (Fig. S9 in ESI†). And the sample taken from TGA/DSC at 800 °C displays an intensive absorption from 600 nm in UV-vis DRS (Fig. 5b), corresponding with the uncontrolled nitridation to TaON and Ta_3N_5 mixtures (Fig. 4). Similar situation is also observed in the case with a $R_{U/Ta}$ of 7.0 (Fig. S8 in ESI†). SrTa/U ($R_{U/Ta} = 7.0$) obviously displays the accelerated nitridation at lower temperature than that of Ta/U due to the mediation of $SrTa_4O_{11}$. This effectively restricts the over-nitridation to TaN that is usually observed in the absence of Sr^{2+} (Fig. 4).

Based on the above results, we propose a new mechanism associated with crucial strontium-tantalate intermediates for controlled nitridation (Scheme 1). In the intermediate of $SrTa_4O_{11}$, parts of Ta-O bonds are weakened. This benefits the replacement of O by N for generating TaON with a low $R_{U/Ta}$, and more importantly avoids over-nitridation to Ta_3N_5 because the residual Ta-O bonds are not affected by Sr^{2+} . In the case with a high $R_{U/Ta}$, the promoted nitridation at $T < 700$ °C also prevents products from over-reacting to TaN. Thus, the controlled nitridation is successfully achieved. In this way, the Sr/Ta ratio controlling the intermediates of tantalates makes obvious influence the generation of TaON and Ta_3N_5 (Fig. S10 in ESI†).

This mechanism is universal for ionothermal processes using other alkaline-earth metal ions. In the presence of Ba^{2+} , TaON and Ta_3N_5 phases are obtained as $R_{U/Ta} = 2.0$ and 5.0, respectively (Fig. S11 in ESI†). Similar pure Ta_3N_5 is fabricated



Scheme.1 Proposed mechanism via a vital strontium-tantalate intermediate for controlled nitridation.

at $R_{U/Ta} = 5.0$ with Ca^{2+} or Mg^{2+} , however, the intermediates of $Ca_2Ta_2O_7$ and $MgTa_2O_6$ still remain at the low $R_{U/Ta}$ of $1.0 \sim 3.0$ (Fig. S12 and S13 in ESI[†]), whose decomposition usually requires complete nitridation with high temperature (> 775 °C) and flow rate (> 1.0 L/min).²⁸ Such difference is probably related to their diverse ionic radius (Mg^{2+} 89 pm; Ca^{2+} 112 pm; Sr^{2+} 126 pm; Ba^{2+} 142 pm).³³ Owing to the toxicity of Ba^{2+} and the difficult decomposition of Ca^{2+} and Mg^{2+} -based tantalates, the Sr^{2+} -mediated route is suitable for the environment-friendly and facile synthesis of nitrides.

We believe that this explanation would make a progress in discovering the essential effects of ionic solvents. Ionothermal routes were ever conducted to fabricate ternary metal oxynitrides, e.g., $MTaO_2N$ ($M = Ca, Sr$ or Ba), $MNbO_2N$ ($M = Sr$ or Ba), however, their functions in controlled nitridation were unfortunately ignored.³⁴ In our previous work,²⁸ the indispensable effect of Ca^{2+} in the controlled synthesis of TaON and Ta_3N_5 was ascribed to the chelation between Ca^{2+} and urea, which slowed down the release of NH_3 from urea decomposition to control nitride generation. However, it cannot elucidate how the urea decomposition at low temperature (< 400 °C) affects nitridation at high temperature (~ 775 °C). Herein, tantalate intermediates are found in the ionothermal routes with a wide range of alkaline-earth-metal salts (e.g., Mg^{2+} , Ca^{2+} , Sr^{2+} and Ba^{2+}), which are indispensable to achieve the well-defined tantalum (oxy)nitrides. The controlled nitridation due to the weakened Ta-O bonds of tantalates successfully protects the desired generations of TaON and Ta_3N_5 from over-reactions, opening new mind in the understanding of ionothermal synthesis.

3.3 Metal-support interactions associated with controlled nitridation

Supported gold has recently emerged as versatile catalysts for a broad array of organic transformations, including a number of hydroprocessing reactions, in which the performance depends on its interactions with supports.^{13,14,35} Given the obviously varied electronic feature in tantalum (oxy)nitrids (*cf.* Fig. 3), metal-support interactions with gold nanocatalysts are expected to be tailored by controlled nitridation. In this regard, Au/Ta_2O_5 , $Au/TaON$ and Au/Ta_3N_5 with an Au loading of $0.8 \sim 0.9\%$ were prepared via a same deposition-precipitation method. As shown in the TEM images (Fig. 6), Au nanoparticles with a uniform size around 3.5 nm are observed on the supports of Ta_2O_5 , TaON and Ta_3N_5 .

H_2 -TPR and XPS analysis were further conducted on the above catalysts. In H_2 -TPR results (Fig. 7a), the strong metal-support interactions in $Au/TaON$ and Au/Ta_3N_5 are suggested by the lower reduction temperature of Au^{3+} species in comparison with Au/Ta_2O_5 , all of which possess the consistent size-distribution of Au (Fig. 6). Although parallel reductions peaking at $121 \sim 122$ °C are both detected, the onset temperature of 72 °C in Au/Ta_3N_5 is lower than that in $Au/TaON$ (97 °C). Such interactions are further affirmed by XPS (Fig. 7b). The sample of Au/Ta_2O_5 displays the Au $4f_{7/2}$ and $4f_{5/2}$ peaks located at 87.6 and 83.9 eV, which are coincident with those for metallic gold.³⁶ With the nitridation of Ta-based

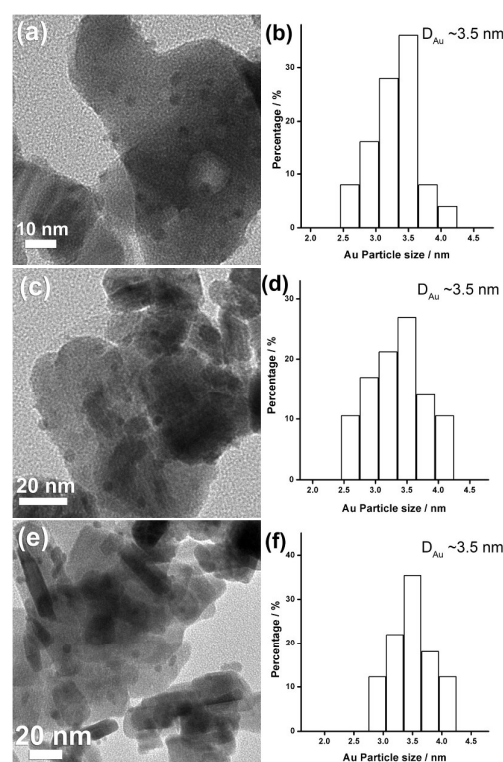


Fig. 6 TEM images of (a) 0.9% Au/Ta_2O_5 , (c) 0.8% $Au/TaON$, (e) 0.9% Au/Ta_3N_5 , and the corresponding size distribution of Au on (b) Ta_2O_5 , (d) TaON, (f) Ta_3N_5 .

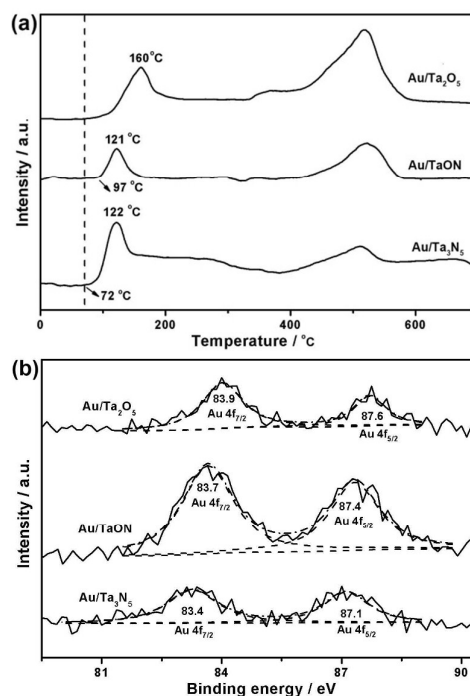


Fig. 7 (a) H_2 -TPR profiles and (b) Au 4f XPS spectra of 0.9% Au/Ta_2O_5 , 0.8% $Au/TaON$, and 0.9% Au/Ta_3N_5 .

supports, these peaks are respectively shifted to the lower binding energies of 87.4 and 83.7 eV in Au/TaON, indicating negatively charged Au species ($\text{Au}^{\delta-}$). This observation should be attributed to the increased Fermi level in nitrated supports (Fig. S4b in ESI[†]), which promotes electron transfer from supports to Au.³⁷⁻³⁹ In Au/Ta₃N₅, the corresponding ones with an obvious red-shift to 87.1 and 83.4 eV suggest that electrons are further accumulated on $\text{Au}^{\delta-}$ surface due to the highly nitrated Ta₃N₅ supports. Such metal-support interactions varied by the nitridation of Ta-based supports are expected to make obvious influence on the catalytic performance of gold.^{40,41}

3.4 Nitrobenzene hydrogenation

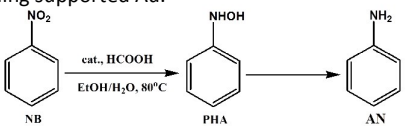
The hydrogenation of nitrobenzene (NB), key routes towards important intermediates for dyestuff, pharmaceuticals, and food additives, is considered as an available probe reactions to identify the function of metal-support interactions due to its multiple steps and directions.⁴² In this work, NB hydrogenation was conducted over Au/Ta₂O₅, Au/TaON and Au/Ta₃N₅ using formic acid (FA) as a safe and economic hydrogen source.⁴³ As shown in Table 1, phenylhydroxylamine (PHA) and aniline (AN) are the products, without nitrosobenzene or azobenzene being detected. A consecutive hydrogenation pathway is suggested, similar with that proposed on Au/TiO₂ by Corma et al.⁴² All the supported Au catalysts show obviously higher activity than bare Ta-based nanoparticles (Entries 1~3 and 4~6 in Table 1), indicating Au as the predominant active species. The catalyst of 0.9%Au/Ta₂O₅ gives a low conversion of 52% with negligible

AN selectivity (Entry 4 in Table 1). The improved activity with an almost complete conversion and a AN selectivity of 51% is achieved on 0.8%Au/TaON (Entry 5 in Table 1), which is superior to those on 0.9%Au/Ta₃N₅ and even on typical 0.8%Au/SiO₂ (Entries 6 and 7 in Table 1). With other Au loading (0.5 ~ 2.0 wt%), the Au/TaON also presents a better activity than that on Au/Ta₂O₅ and Au/Ta₃N₅ (Table S2 in ESI[†]), suggesting a high activity associated with the TaON support. It can be further confirmed by NB reduction using H₂, which shows analogous situation (Entries 8~10 in Table 1). Additionally, the AN selectivity on Au/TaON can be improved by increasing Au loading (Entries 5 and 11-13 in Table 1), agreeing with the nature of consecutive hydrogenation pathway.

Considering the similar catalytic FA decomposition to CO₂ and H₂ over Au/Ta₂O₅, Au/TaON and Au/Ta₃N₅ (Table S3 in ESI[†]), the different performance for NB reduction by FA should be contributed by the reduction steps of NB. Further test in the direct hydrogenation of PHA exhibits the negligible difference (Table S4 in ESI[†]), suggesting the varied activity in the first step from NB to PHA. The intrinsic properties of Au in the above catalysts are believed as a key factor for NB hydrogenation, regarding the similarities in surface area, Au particle size and active-site amount already confirmed by N₂ sorption analysis, TEM investigation and CO uptake experiment, respectively (Table S1 in ESI[†] and Fig. 6).

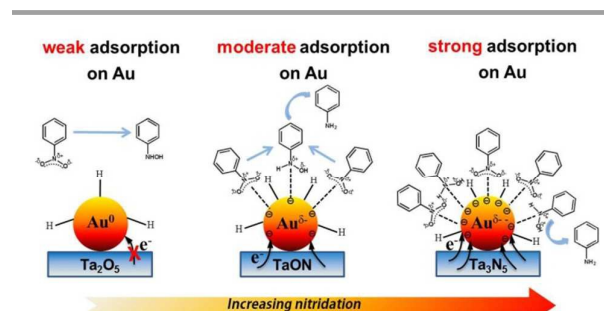
Typically, the adsorption of NB substrate on Au is the key in NB reduction.^{44,45} According to the Balandin-type volcano plots, the moderate adsorption on metals is demanded for efficient catalytic conversion because a weak adsorption cannot effectively activate substrates and a strong adsorption precludes product desorption.^{46,47} Negatively charged $\text{Au}^{\delta-}$ over TaON resulting from electronic metal-support interactions^{38,39} (c.f. XPS in Fig. 7b) would promote the adsorption of polar $-\text{N}^{\delta+}-\text{O}^{\delta-}$ bonds in NB,^{42,46,47} as compared with the neutral Au on Ta₂O₅, which presents optimized activity and selectivity (Scheme 2). As for Au/Ta₃N₅, the further negatively charged $\text{Au}^{\delta-}$ on Ta₃N₅ would make NB and even as-formed PHA adsorption so strong that the following steps are hindered.⁴⁶ And thus, the reduced activity and AN selectivity are observed. Obviously, an appropriate nitridation level of supports is critical for optimizing metal-support interactions with gold nanocatalysts.

Table 1. Hydrogenation of NB over Ta-based nanoparticles and the corresponding supported Au.



Entry	Catalyst	Conv.(%)	Sel. (%)	
			PHA	AN
1	Ta ₂ O ₅ ^[a]	33	>99	0
2	TaON ^[a]	30	>99	0
3	Ta ₃ N ₅ ^[a]	35	>99	0
4	0.9% Au/Ta ₂ O ₅ ^[a]	52	92	8
5	0.8% Au/TaON ^[a]	>99	49	51
6	0.9% Au/Ta ₃ N ₅ ^[a]	73	60	40
7	0.8% Au/SiO ₂ ^[a]	74	83	17
8	0.9% Au/Ta ₂ O ₅ ^[b]	52	>99	0
9	0.8% Au/TaON ^[b]	65	>99	0
10	0.9% Au/Ta ₃ N ₅ ^[b]	58	>99	0
11	0.5% Au/TaON ^[a]	39	85	15
12	1.3% Au/TaON ^[a]	>99	29	71
13	1.7% Au/TaON ^[a]	>99	27	73

[a] Typical conditions: NB (0.5 mmol), catalysts (40 mg), FA (6.0 mmol), EtOH (5.0 mL), H₂O (5.0 mL), N₂ (0.5 MPa), 80 °C, 2.5 hours. [b] H₂ (0.5 MPa) was used as the reductant.



Scheme 2. Schematic illustration for NB hydrogenation over Au/Ta₂O₅, Au/TaON and Au/Ta₃N₅.

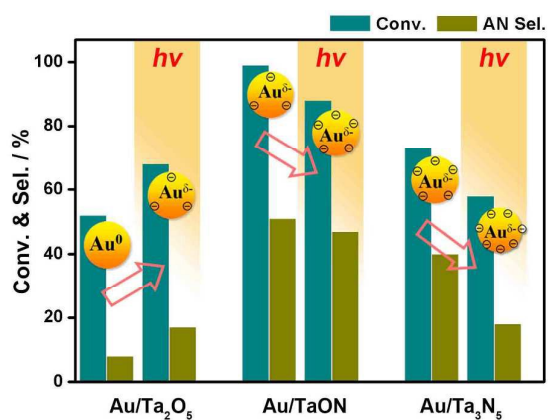


Fig. 8 Comparison of NB hydrogenation over Ta-NPs supported Au with and without light irradiation.

Another test under light irradiation, showing further affected charge-distribution on Au by photo-excited electrons, can serve as an important evidence for the above conclusion in nonphotocatalytic condition. In view of the different band-gap energy of Ta₂O₅, TaON and Ta₃N₅, UV ($\lambda > 200$ nm) and visible ($\lambda = 400 \sim 800$ nm) light was employed for Au/Ta₂O₅ and the both of Au/TaON and Au/Ta₃N₅, respectively. The increased activity is observed on Au/Ta₂O₅, while the decreased one is presented by Au/TaON and Au/Ta₃N₅, in contrast with that without irradiation (Fig. 8). Thanks to the excited electron from Ta₂O₅ to Au, the as-formed Au^{δ-} accelerates NB reduction by enhanced adsorption. However, too strong NB and PHA adsorption on excessively charged Au^{δ-}, strengthened by photo-excitation, would block the following reactions and thus reduce the activity on Au/TaON and Au/Ta₃N₅. Additionally, the test under visible light ($\lambda = 400 \sim 800$ nm) was also conducted on Au/Ta₂O₅. The performance similar to that without irradiation, but lower than that with UV, should be ascribed to the failure to excite wide-band-gap Ta₂O₅ (3.9 eV) by visible light. This test eliminates the influence from the visible-light plasmonic effects of Au.

4. Conclusions

A Sr²⁺-mediated ionothermal synthesis with an improved mechanism has been successfully introduced to fabricate tantalum (oxy)nitride nanoparticles with well-defined composition and electronic properties. This work demonstrates a strategy to vary the electronic features of tantalum (oxy)nitrides towards optimized metal-support interactions with Au, which promotes the hydrogenation of NB by controlling the electronic feature of Au and the consequent substrate adsorption/activation. Our effort highlights the advantages of controlled nitridation for achieving optimized metal-support interactions, pointing out a new protocol for catalyst design.

Acknowledgements

This work is financially supported by the National Basic Research Program of China (2013CB934101), National Natural Science Foundation of China (21203075, 21373102, and 21433002) and Fundamental Research Funds for the Central Universities (21615402). Q. S. Gao also thanks the support from Guangdong Natural Science Funds (2015A030306014 and 2014TQ01N036) and Guangdong Higher Education Institute (YQ2013022).

Notes and references

1. A. Salamat, A. L. Hector, P. Kroll and P. F. McMillan, *Coord. Chem. Rev.*, 2013, **257**, 2063-2072.
2. J. S. J. Hargreaves, *Coord. Chem. Rev.*, 2013, **257**, 2015-2031.
3. X. J. Lang, X. D. Chen and J. C. Zhao, *Chem. Soc. Rev.*, 2014, **43**, 473-486.
4. N. E. Breese, *Structure and Bonding, Crystal Chemistry of Inorganic Nitride*, Springer, Berlin, 1992.
5. E. Furimsky, *Appl. Catal. A-Gen.*, 2003, **240**, 1-28.
6. V. Heine, *Phys. Rev.*, 1967, **153**, 673-682.
7. A. M. Alexander and J. S. J. Hargreaves, *Chem. Soc. Rev.*, 2010, **39**, 4388-4401.
8. Q. S. Gao, N. Liu, S. N. Wang and Y. Tang, *Nanoscale*, 2014, **6**, 14106-14120.
9. M. M. O. Thotiyil, T. R. Kumar and S. Sampath, *J. Phys. Chem. C*, 2010, **114**, 17934-17941.
10. V. Molinari, C. Giordano, M. Antonietti and D. Esposito, *J. Am. Chem. Soc.*, 2014, **136**, 1758-1761.
11. N. Perret, F. Cardenas-Lizana, D. Lamey, V. Laporte, L. Kiwi-Minsker and M. A. Keane, *Topics in Catal.*, 2012, **55**, 955-968.
12. F. Cardenas-Lizana, D. Lamey, N. Perret, S. Gomez-Quero, L. Kiwi-Minsker and M. A. Keane, *Catal. Commun.*, 2012, **21**, 46-51.
13. X. Liu, L. He, Y. M. Liu and Y. Cao, *Acc. Chem. Res.*, 2014, **47**, 793-804.
14. A. Corma and H. Garcia, *Chem. Soc. Rev.*, 2008, **37**, 2096-2126.
15. X. H. Li and M. Antonietti, *Chem. Soc. Rev.*, 2013, **42**, 6593-6604.
16. R. Asahi, T. Morikawa, T. Ohwaki, K. Aoki and Y. Taga, *Science*, 2001, **293**, 269-271.
17. K. Maeda and K. Domen, *J. Phys. Chem. C*, 2007, **111**, 7851-7861.
18. R. Abe, M. Higashi and K. Domen, *J. Am. Chem. Soc.*, 2010, **132**, 11828-11829.
19. Y. G. Su, J. Y. Lang, L. P. Li, K. Guan, C. F. Du, L. M. Peng, D. Han and X. J. Wang, *J. Am. Chem. Soc.*, 2013, **135**, 11433-11436.
20. Q. S. Gao, S. N. Wang, Y. C. Ma, Y. Tang, C. Giordano and M. Antonietti, *Angew. Chem. Int. Ed.*, 2012, **51**, 961-965.
21. Q. S. Gao, C. Giordano and M. Antonietti, *Angew. Chem. Int. Ed.*, 2012, **51**, 11740-11744.
22. M. E. Strayer, J. M. Binz, M. Tanase, S. M. K. Shahri, R. Sharma, R. M. Rioux and T. E. Mallouk, *J. Am. Chem. Soc.*, 2014, **136**, 5687-5696.
23. A. Kumar and V. Ramani, *ACS Catal.*, 2014, **4**, 1516-1525.
24. K. An, S. Alayoglu, N. Musselwhite, K. Na and G. A. Somorjai, *J. Am. Chem. Soc.*, 2014, **136**, 6830-6833.

25. E. Orhan, F. Tessier and R. Marchand, *Solid State Sci.*, 2002, **4**, 1071-1076.
26. M. Kerlau, O. Merdrignac-Conanec, M. Guilloux-Viry and A. Perrin, *Solid State Sci.*, 2004, **6**, 101-107.
27. C. Giordano and M. Antonietti, *Nano Today*, 2011, **6**, 366-380.
28. Q. S. Gao, C. Giordano and M. Antonietti, *Small*, 2011, **7**, 3334-3340.
29. W. J. Chun, A. Ishikawa, H. Fujisawa, T. Takata, J. N. Kondo, M. Hara, M. Kawai, Y. Matsumoto and K. Domen, *J. Phys. Chem. B*, 2003, **107**, 1798-1803.
30. X. F. Liu, N. Fechler and M. Antonietti, *Chem. Soc. Rev.*, 2013, **42**, 8237-8265.
31. Z. Schnepf, M. Thomas, S. Glatzel, K. Schlichte, R. Palkovits and C. Giordano, *J. Mater. Chem.*, 2011, **21**, 17760-17764.
32. D. Mitoraj and H. Kisch, *Chem.-Eur. J.*, 2010, **16**, 261-269.
33. J. G. Speight, *Lange's Handbook of Chemistry*, McGraw-Hill Professional, New York, 16 edn., 2005.
34. A. Gomathi, S. Reshma and C. N. R. Rao, *J. Solid State Chem.*, 2009, **182**, 72-76.
35. A. S. K. Hashmi and G. J. Hutchings, *Angew. Chem. Int. Ed.*, 2006, **45**, 7896-7936.
36. P. Kast, G. Kucerova and R. J. Behm, *Catal. Today*, 2015, **244**, 146-160.
37. Y.-N. Sun, L. Giordano, J. Goniakowski, M. Lewandowski, Z.-H. Qin, C. Noguera, S. Shaikhutdinov, G. Pacchioni and H.-J. Freund, *Angew. Chem. Int. Ed.*, 2010, **49**, 4418-4421.
38. X. Y. Liu, A. Q. Wang, T. Zhang and C. Y. Mou, *Nano Today*, 2013, **8**, 403-416.
39. A. M. Kolpak, I. Grinberg and A. M. Rappe, *Phys. Rev. Lett.*, 2007, **98**, 166101.
40. T. Mitsudome and K. Kaneda, *Green Chem.*, 2013, **15**, 2636-2654.
41. S. Schauer mann, N. Nilius, S. Shaikhutdinov and H. J. Freund, *Acc. Chem. Res.*, 2013, **46**, 1673-1681.
42. A. Corma, P. Concepcion and P. Serna, *Angew. Chem. Int. Ed.*, 2007, **46**, 7266-7269.
43. I. Sorribes, G. Wienhofer, C. Vicent, K. Junge, R. Llusar and M. Beller, *Angew. Chem. Int. Ed.*, 2012, **51**, 7794-7798.
44. L. Y. Zou, Y. Y. Cui and W. L. Dai, *Chin. J. Chem.*, 2014, **32**, 257-262.
45. M. Boronat, P. Concepcion, A. Corma, S. Gonzalez, F. Illas and P. Serna, *J. Am. Chem. Soc.*, 2007, **129**, 16230-16237.
46. M. Turakova, T. Salmi, K. Eraenen, J. Waerna, D. Y. Murzin and M. Kralik, *Appl. Catal. A-Gen.*, 2015, **499**, 66-76.
47. L. Zhang, J. Jiang, W. Shi, S. Xia, Z. Ni and X. Xiao, *RSC Adv.*, 2015, **5**, 34319-34326.